AIAA JOURNAL
Vol. 34, No. 12, December 1996

Effects of Leading-Edge Lateral Blowing on Delta Wing Aerodynamics

John S. Hong*
Institute for Defense Analyses, Alexandria, Virginia 22311-1772
and
Zeki Z. Çelik† and Leonard Roberts‡
Stanford University, Stanford, California 94305

An experimental and computational study was carried out to investigate the effects of lateral blowing on a delta wing at low to moderate angles of attack. Motivation for the present study is to use lateral blowing to increase lift and to provide roll control for a high-speed configuration during takeoff and landing approaches. For this purpose, lateral blowing was applied through blowing slots along the leading edge of a delta wing symmetrically to increase lift and asymmetrically to induce rolling moments. Experiments showed that the higher the blowing rate, the greater the forces and moments that were attained on the model. Results also showed that the effect of blowing on the strength and location of the vortex sheet depended on the strength of the jet and the angle of attack. Computed solutions of the Navier–Stokes equations were obtained for the same wing geometry. Computations successfully captured the qualitative trends observed in the experiments. The physics of the blowing scheme, the underlying mechanisms of the control reversal phenomenon, and the higher efficiency of partial slot blowing compared with full slot blowing were determined by both examining the experimental and computational results.

Nomenclature

A_j = blowing slot area
AR = aspect ratio
C_l = roll moment coefficient
C_N = normal force coefficient
C_μ = jet momentum coefficient, $\dot{m}_j V_j / 0.5 \rho_\infty V_\infty^2 S$
c = root chord length
l = blowing slot length
$\dot{m}_j$ = jet mass flow rate, $\rho_j V_j A_j$
Re = Reynolds number
S = wing platform area
s = span of the model
t = blowing slot height
V_j = jet velocity
V_∞ = freestream velocity
α = angle of attack
β = jet ejection angle
Δ = difference between blowing and no blowing cases
ρ = density of air
ϕ = roll angle

Introduction

THE aerodynamics of delta wings are dominated by the vortical flowfield established by the leading-edge vortices. These vortices generate a significant nonlinear lift increment, generally called the vortex-induced lift. Because these vortices play such a significant role, it is desirable to alter and to control their development to further enhance their favorable influence. Research has shown that additional aerodynamic forces and moments can be obtained by pneumatic means through the change of the leading-edge vortex strength and position. In this work, the manipulation of the leading-edge vortex is accomplished by using leading-edge lateral blowing. The use of lateral blowing to augment lift on straight and delta wings has been reported in various references.[1–8] Lateral blowing is applied by extending a blowing slot along the leading edge of the delta wing and ejecting a thin jet laterally. The momentum injected into the flowfield alters the equilibrium of the vortical flow system and changes the strength and location of the vortex sheet. Depending on the blowing configuration that may be symmetrical or asymmetrical, the new flowfield can generate higher lift and/or rolling moment.

In this research, the effects of leading-edge lateral blowing were investigated experimentally[9] on a delta wing by means of smoke and surface oil flow visualization, force and moment measurements, and total and surface pressure measurements and computationally[10] by solving the Navier–Stokes equations. Motivation for this research is that there is a need for a clean high lift and roll mechanism, that is, a control device that would generate aerodynamic control forces without the intervention of deflecting solid surfaces and would give no drag penalty when not in use, allowing high-speed configurations to fly at low speeds with sufficient lift and controllability during takeoff and landing approaches. The objective of this paper is to study and to understand the aerodynamics behind this blowing scheme and to demonstrate its feasibility and effectiveness as a lift and roll control mechanism.

Experimental Apparatus

Wind Tunnel and Model

Experiments were conducted in the Stanford University low-speed wind tunnel. The test section is 0.45 × 0.45 m, and the model was tested at nominal velocities of 25 and 40 m/s, which approximately correspond to the Reynolds numbers of 3.25×10^5 and 5×10^5 based on the root chord length. A schematic of the model, which shows the dimensional characteristics, is illustrated in Fig. 1. The thickness of the delta wing varies linearly from zero at the tip to a finite value of $0.247c$ at the trailing edge. It has two separate plena from which blowing can be administered independently through the tapered slots on each side along the leading edge of the wing. With this configuration, it is possible to apply blowing symmetrically from both plena to augment normal force or asymmetrically from either slot to induce a rolling moment as well as increasing the normal force. Blowing slots on the wing section were located along the leading edges, and the slot opening was tapered to conserve the properties of conical flow, observed in flows around delta wings. For full slot blowing, the slot length was $0.91c$ long with a slot opening of $2.6 \times 10^{-4}c$ at the tip and $3.3 \times 10^{-3}c$ at the trailing edge. For partial blowing, the front portion of the blowing slot was covered

Received Oct. 24, 1995; revision received May 8, 1996; accepted for publication Aug. 9, 1996; also published in *AIAA Journal on Disc*, Volume 2, Number 1.

*Research Staff, System Evaluation Division, 1801 N. Beauregard Street. Member AIAA.
†Research Associate, Department of Aeronautics and Astronautics. Member AIAA.
‡Professor, Department of Aeronautics and Astronautics. Fellow AIAA.

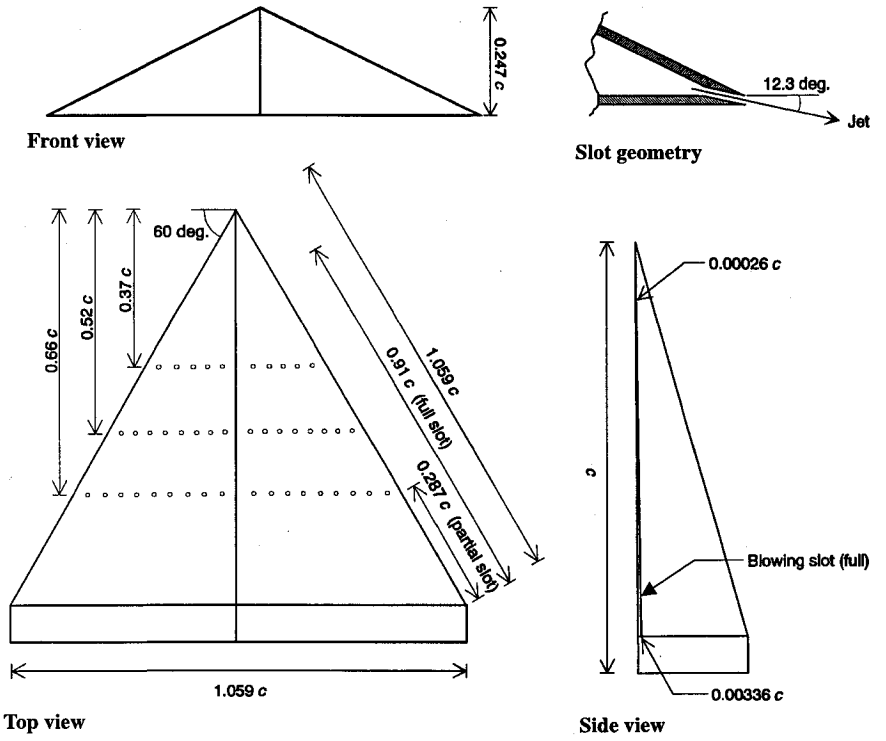

Fig. 1 Schematic of the model with dimensional characteristics.

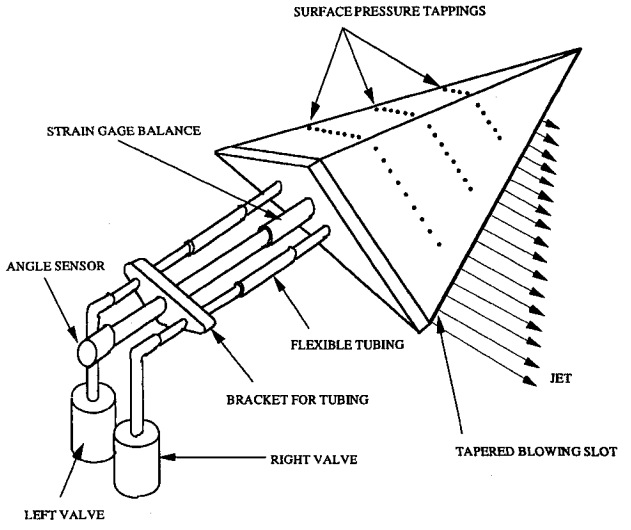

Fig. 2 Schematic of the mounting configuration of the model.

on both sides. The partial slot opening was $0.287c$ long, and the effective area was approximately half of the full blowing area. The aspect ratio AR of the wing is 1.95 as referenced to the platform area, and the ejection angle of the jet β is 12.3 deg downward with respect to the wing bottom surface.

Instrumentation

There were 44 pressure tappings distributed at three chordwise locations on the upper surface of the model. No pressure tappings were attached on the bottom surface of the wing. Pressure readings were taken through a Scanivalve unit and processed on a personal computer equipped with a data acquisition card. A pitot tube was also utilized to take total pressure measurements.

In the smoke flow visualization experiments, a laser sheet was directed to the model in such a way that it was perpendicular to the bottom surface. Smoke flow visualization tests were conducted at a velocity of 8 m/s, which corresponded to a Reynolds number of 10^5. Surface oil visualization experiments were carried out at a test section velocity of 25 m/s. The model was mounted on a three-component strain gauge balance to measure normal force, pitching moment, and rolling moment. Air inlet hoses were located at the base of the model, as shown in Fig. 2.

Data Acquisition

The jet blowing momentum coefficient C_μ was defined as the ratio of jet momentum to the product of dynamic pressure and reference area. The jet momentum was calculated from the incompressible Bernoulli equation using plenum pressure measurements and by assuming that the jet exit pressure is equal to the local static pressure of the flow. The strain gauge balance was calibrated wind-off, and the interference between the force and moments were accounted for in the balance calibration matrix. Pressure transducers of the Scanivalve system were calibrated before each run. Wall interference effects were not taken into account by considering that the test angles were small and by assuming that the blowing would not change the initial interference significantly.

Computational Method

Governing Equation and Flow Solver

The flow solver used in the study was OVERFLOW, developed at the NASA Ames Research Center.[11] The code is a general purpose three-dimensional Reynolds-averaged compressible Navier–Stokes flow solver. Several numerical schemes are available as options in the code. The implicit three-factor diagonalized Beam–Warming scheme was chosen due to its reduced operation count for steady-state problems. To accelerate convergence, a minimum Courant–Friedrichs–Lewy number limit was used to expedite the process of setting up the inviscid portion of the flow, which in turn drives the boundary-layer flow. In addition, a spatially varying time step was used to further speed up convergence. An algebraic turbulence model developed by Baldwin and Lomax[12] and later modified by Degani and Schiff[13] for application to three-dimensional flows with crossflow separation was used for turbulence closure.

Grid Generation

The geometry and dimensions of the computational model were chosen to match those of the model used in the wind-tunnel experiments. The surface grid was generated algebraically using a stretching method by Vinokur[14] to provide adequate resolution of the jet slots and to capture the rapid changes around the convex corners.

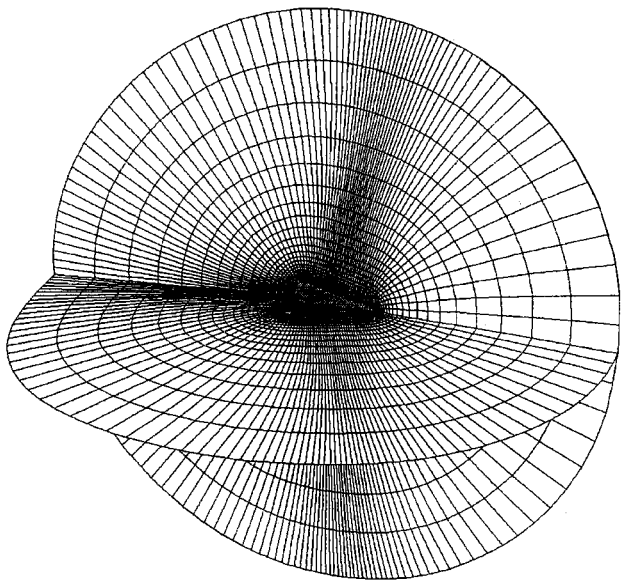

Fig. 3 Computational grid.

The volume grid was generated using the hyperbolic grid generator HYPGEN developed at the NASA Ames Research Center. The topology of the grid is O-O, and the radius of the cross section is three chord lengths. In the computations, three grids were used. The first grid is a half-span delta wing, which was used for the symmetric computations and consists of 77 × 98 × 59 grid points. This grid is shown in Fig. 3. The full-span grid used for the asymmetric computations consists of 77 × 191 × 59 grid points. A grid resolution study was also conducted using a finer grid of the half-span wing with twice as many points, 97 × 124 × 74, and has shown that the numerical solution is grid independent.

Boundary Conditions

The wall boundary conditions were set at a no-slip, adiabatic condition, and for the outflow boundaries, characteristics based conditions were imposed. For the half-span computations, a symmetric plane boundary condition was used, whereas for full-span computations, a periodic boundary condition was applied at the half-plane to allow for asymmetric flow. Because of the two polar grids used at the wing apex and trailing edge, two axial conditions were also required. For computational purposes, the jet is usually implemented as a one-sided source of mass, momentum, and energy.[8] For the leading-edge lateral blowing case, the jet characteristics were calculated using the blowing coefficient C_μ. The jet conservative flow variable vector was then specified explicitly at a zonal boundary that matches the height, length, and location of the experimental jet slot.

Results and Discussion

Experiments and computations were carried out at varying blowing rates and angles of attack. The angle of attack of the model was defined with respect to the bottom surface of the model and did not represent the actual angle of attack that would be defined relative to the zero-lift line. In the experiments, normal force, pitching moment, and rolling moment were measured at angles of attack from 0 to 30 deg. Surface and total pressure measurements were taken at several locations on the model, $x/c = 0.37$, 0.52, and 0.66 at $\alpha = 10$ and 20 deg. Blowing from a partial slot was also applied to compare its effectiveness with full slot blowing. Visual assessment of the effects of lateral blowing on the model was accomplished by smoke and surface oil flow visualization. Smoke flow visualization experiments were carried out at $\alpha = 5$, 7.5, 10, and 20 deg. Surface oil flow experiments were done at $\alpha = 10$ and 20 deg with $C_\mu = 0$, 0.03, and 0.06. Numerical solutions were obtained using the same freestream conditions of the experiments. Computational solutions were sought for angles of attack of 10, 20, and 30 deg with blowing coefficients of $C_\mu = 0$, 0.01, 0.03, and 0.06 using both symmetric and asymmetric blowing for comparison with the experimental data and to enhance the understanding of the aerodynamics behind leading-edge lateral blowing.

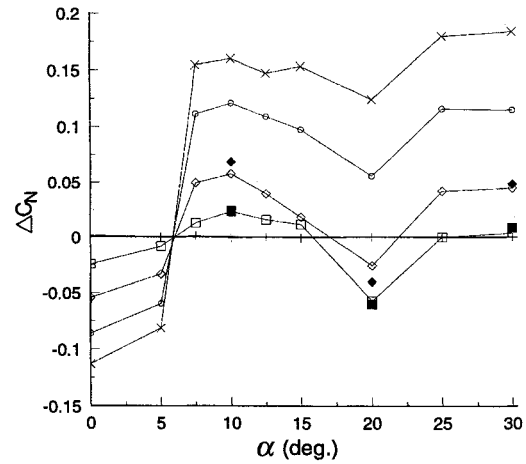

Fig. 4 Experimental and computational results of normal force augmentation. Experiments: +, C_μ = 0; □, C_μ = 0.01; ◇, C_μ = 0.03; ○, C_μ = 0.06; and ×, C_μ = 0.06. Computations: ■, C_μ = 0.01 and ♦, C_μ = 0.03.

Aerodynamic Force Augmentation and Control Reversal

Symmetrical blowing was applied to the wing to explore its potential as a lift augmentation device. To isolate the effect of lateral blowing, the no blowing case was used as a base for comparison. Figure 4 shows the experimental results of the variation in the normal force coefficient ΔC_N as a function of angle of attack and C_μ. Because the computations were time consuming and costly, only a couple of cases that were important for the analysis were computed and are shown in Fig. 4 for comparison. The variation of the normal force coefficient was found to be a function of the blowing jet strength and angle of attack. For angles of attack less than approximately 6 deg, the normal force coefficient decreases as the jet strength increases. This is because of the formation of the leading-edge vortex on the bottom of the wing, which was confirmed by smoke flow visualization. The blowing jet sheet rolls down and strengthens these vortices, which pull the wing down. However, for angles of attack larger than 6 deg, the vortices form above the wing, and with the exception of an angle of attack of 20 deg, the normal force increases with the increasing strength of the symmetrical blowing jets. At the angle of attack of 20 deg, a transition of flow characteristics appears to occur. The normal force actually decreases for blowing coefficients equal to or smaller than 0.03 and then increases for larger blowing coefficients. This control reversal phenomenon is quite troublesome and undesirable. To reduce this nonlinear behavior and to use leading-edge blowing effectively, the underlying physics of this problem must be understood. By analyzing the experimental and computational results, its mechanism was determined and will be explained in the following sections. Throughout the angle-of-attack range of interest, three angles of attack, $\alpha = 10$, 20, and 30 deg, were examined with particular interest because distinct flow structures developed under lateral blowing as found experimentally.

The computed surface pressure distributions at four downstream stations at an angle of attack of 10 deg are given in Fig. 5. For the no blowing case, measured and computed pressure distributions along the delta wing and flow visualization experiments show that there is almost no vortical flow structure at this low angle of attack. The pressure distributions show that once blowing is applied, a leading-edge vortex is formed. This is because vorticity from the jet feeds the vortex structure and strengthens it. This vortex formation can be seen more dramatically from the total pressure contours in Fig. 6. Because a jet sheet can sustain a pressure difference, as the blowing momentum increases, the effective span of the wing widens, which in turn moves the vortex position outboard and increases the vortex suction peak. Total pressure measurements, as given in Fig. 7, confirm these observations. It can also be seen that the pressure distribution does not change near the root chord, showing that lateral

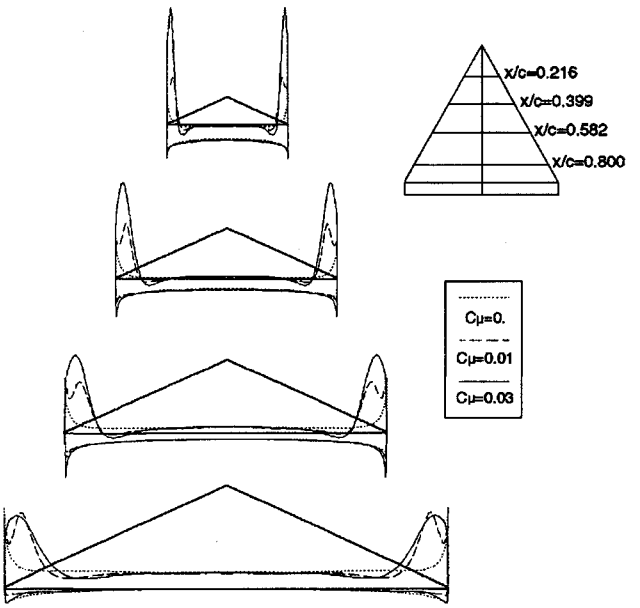

Fig. 5 Computed surface pressure distribution (α = 10 deg).

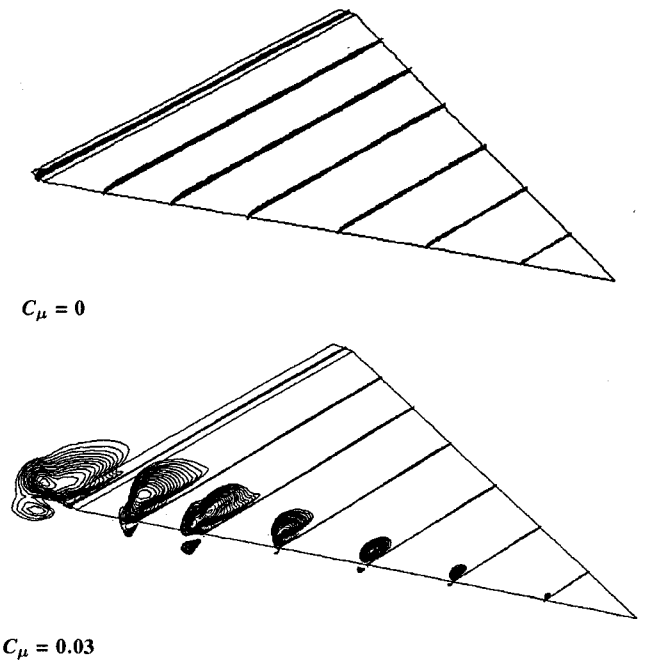

Fig. 6 Computed total pressure contours (α = 10 deg).

blowing only affects the vortex structure and hence the vortical lift. The oil flow patterns from both the experiments and computations are compared in Fig. 8 at an angle of attack of 10 deg with blowing coefficients $C_\mu = 0.0$ and 0.03. For the no blowing case, only the primary attachment line is present, and there are no secondary or tertiary separation lines. The computational attachment line location matches very well with the experimental results. The rapid change in diverging streamlines, for the blowing case, indicates that the vortex strength has increased. A separation line is observed near the leading edge. However, the experimental results show that this line lies further inboard than what the computational results show.

At an angle of attack of 20 deg, experimental and computational results indicate that the control reversal phenomenon occurs. As shown in Fig. 4, at $C_\mu = 0.01$, the normal force on the wing decreased significantly, and although the $C_\mu = 0.03$ case has a larger normal force, it is still below the no blowing level. Computations capture this effect well, and the surface pressure distribution in Fig. 9 helps to explain this occurrence. For an angle of attack of 20 deg,

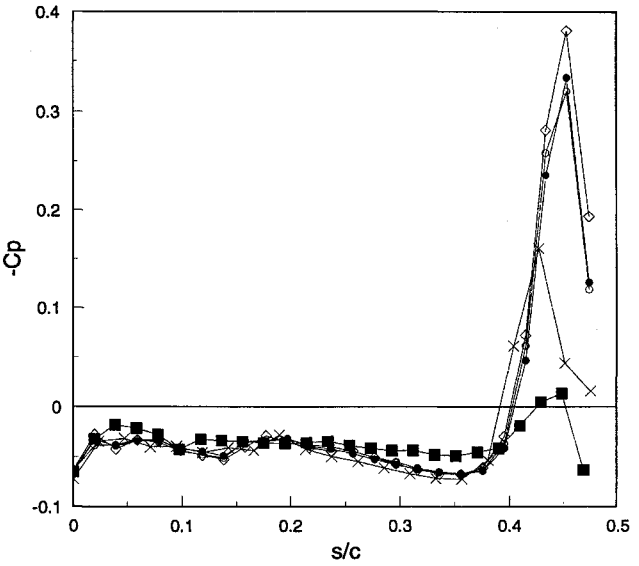

Fig. 7 Total pressure measurements near the wing surface for the asymmetrical blowing case (α = 10 deg and x/c = 0.66): ■, C_μ = 0; ×, C_μ = 0.02; ●, C_μ = 0.042; ○, C_μ = 0.042 (symmetrical); and ◇, C_μ = 0.061.

there is a vortical structure even without blowing. As blowing is applied, both the primary and the secondary vortices increase in strength near the apex as the blowing momentum increases, and both vortices move outboard. It is observed that vortex breakdown does occur near the trailing edge where the span is larger, and hence there is more surface area affected by the vortex bursting. This vortex breakdown can be attributed to the fact that blowing increases the vortex strength, and therefore the adverse pressure gradient along the core becomes more pronounced near the trailing edge, which in turn encourages vortex bursting. Furthermore, the angle of attack at which vortex breakdown occurs decreases as the aspect ratio of the wing increases. Because the jet increases the effective apex angle, vortex breakdown occurs at lower angles of attack. The vortex breakdown is more severe for the larger blowing momentum case, and there is a significant loss of suction force on the upper surface of the wing. However, the higher blowing momentum case, $C_\mu = 0.03$, already had a large increase of normal force near the apex. The overall effect is a loss of normal force compared with the no blowing case, but nevertheless an increase compared with the case of $C_\mu = 0.01$. The total pressure contours at the trailing edge are compared between the experiments and computations in Fig. 10 to ensure that the computations are capturing the flow features observed in the experiments properly. The scales used for the total pressure contours are identical for easy comparison. The computations capture the primary vortex strength and position for the no blowing case and the burst vortex characteristics for the blowing case quite accurately.

As the angle of attack is increased to 30 deg, the normal force increases again with lateral blowing. This occurrence can be explained by the surface pressure distributions in Fig. 11. Because of the high angle of attack, the vortex breaks down near the trailing edge even without blowing. Again, near the apex, blowing strengthens both the primary and secondary vortices and also moves them outboard. The vortex soon breaks down, and there is a loss of the suction peaks. However, unlike the α = 10 and 20 deg cases, the area near the root chord is also affected. This compensates for the loss in the suction peaks. It can be observed by looking at stations 3 and 4 in Fig. 11 that leading-edge lateral blowing can actually strengthen the burst vortex at locations where the vortex would have burst without blowing. The increase of lift near the root chord also continues downstream.

An examination of the experimental and computational results allows a more thorough explanation of how lateral blowing affects the flow structure and augments the aerodynamic forces and moments. First, because the jet sheet velocity is larger than that of the surrounding flow, vorticity is created near the jet sheet boundary. The vorticity on top of the jet sheet feeds into the leading-edge vortex

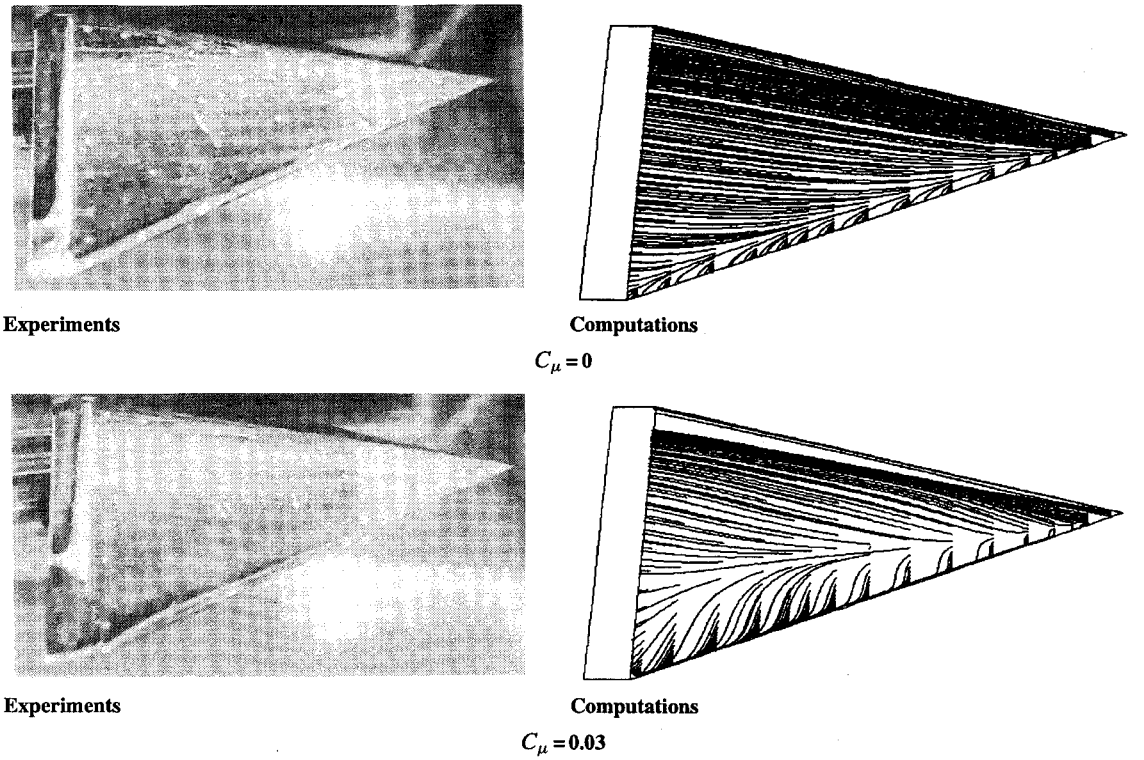

Fig. 8 Comparison of oil flow patterns between experiments and computations (α = 10 deg).

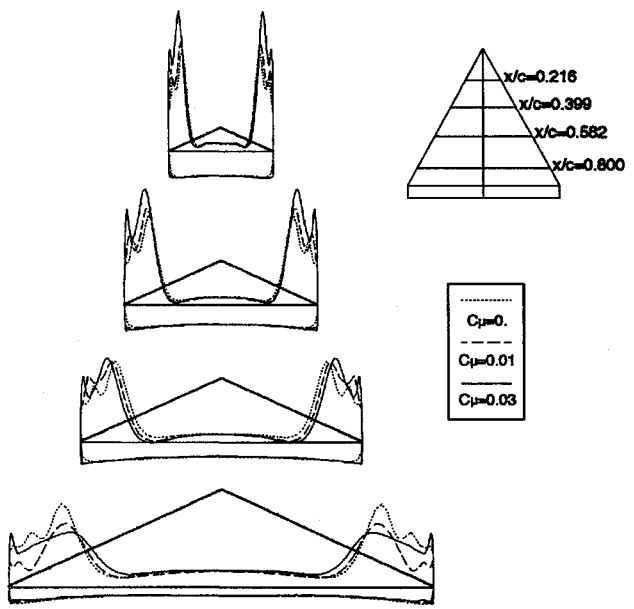

Fig. 9 Computed surface pressure distribution (α = 20 deg).

and strengthens it and therefore increases the suction on the top of the wing. The vorticity below the jet sheet forms a weak vortex with an opposite direction. Once this vortex goes past the blowing slots, it either merges with the primary vortex near the trailing edge or moves downstream and dissipates. Second, the effective span of the wing is increased because a jet sheet can sustain a pressure difference. This increase of the apex angle not only strengthens the vortex but also moves its position outboard. Finally, because the jet sheet has a slight downward component, there is a small direct jet momentum contribution of $C_\mu \sin \beta$.

Rolling Moment Generation

One of the primary purposes of the present study was to explore the possibility of using asymmetrical lateral blowing as a roll control device. In the experiments, asymmetrical blowing from either side of the delta wing induced rolling moments. Force and pressure measurements under asymmetrical blowing configurations showed that blowing on one side of the wing did not significantly affect the flow on the opposite side. This uncoupling can be seen from the experimental results shown in Fig. 7, where the symmetrical and asymmetrical blowing at $C_\mu = 0.042$ produced nearly identical pressure distributions. Figure 12 demonstrates this ability of lateral blowing to generate rolling moments. The rolling moment coefficient is given as a function of the right jet momentum and the angle of attack. The variation of the rolling moment is consistent with the variation in the normal force that was discussed previously. In most cases, lateral blowing increased the vortex strength on the same side and in turn generated more suction to generate the rolling moments. However, at some angles, mainly $\alpha = 15, 20$, and 25 deg, and at low blowing rates, the rolling moment changed sign. The reason for this roll reversal is the same as the arguments presented in the previous section, which explained the normal force reversal.

Blowing Effectiveness at a Bank Angle

The effect of blowing on the rolling moment coefficient at a given roll angle remains as effective as it is at $\phi = 0$ deg. Experimental data given in Fig. 13 indicate that the variation in the rolling moment ΔC_l can fall in a well-defined band of curve as plotted from $\phi = 2$–10 deg at $\alpha = 12.5$ deg when lateral blowing was applied from the right side. This is particularly important if one would want to implement lateral blowing for trim control. The same trend was observed when blowing was applied from the left side and also at other angles of attack.

Partial Slot Blowing

The mass flow required for lateral blowing can be acquired as the bleed air from the jet engines. Because the engine compressor bleed air is typically used for environmental control and to cool avionics, one would like to generate the required forces and moments as efficiently as possible, i.e., with minimum mass flow rate. Moreover, the presence of a blowing slot along the entire leading edge may not be an acceptable design consideration. The alternative was to apply the blowing from a partial slot. Therefore, two slot configurations, the full slot and the partial slot, were studied. Partial blowing

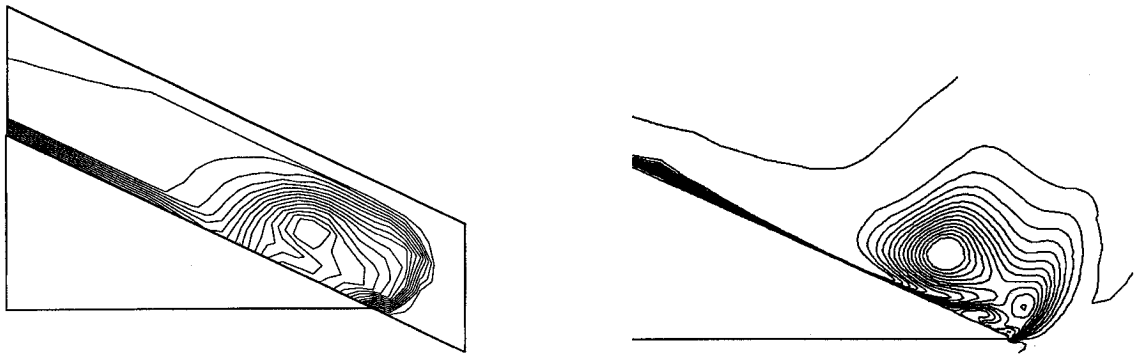

Experiments Computations

$C_\mu = 0$
(scale: $-1.324 \sim 0.768$ in 0.149 intervals)

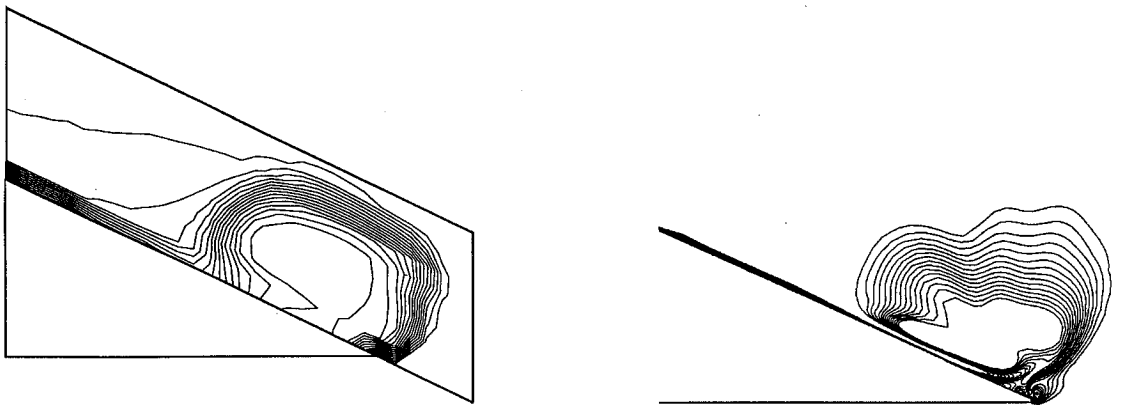

Experiments Computations

$C_\mu = 0.03$
(scale: $-1.253 \sim 0.635$ in 0.135 intervals)

Fig. 10 Comparison of total pressure contours between experiments and computations (α = 20 deg).

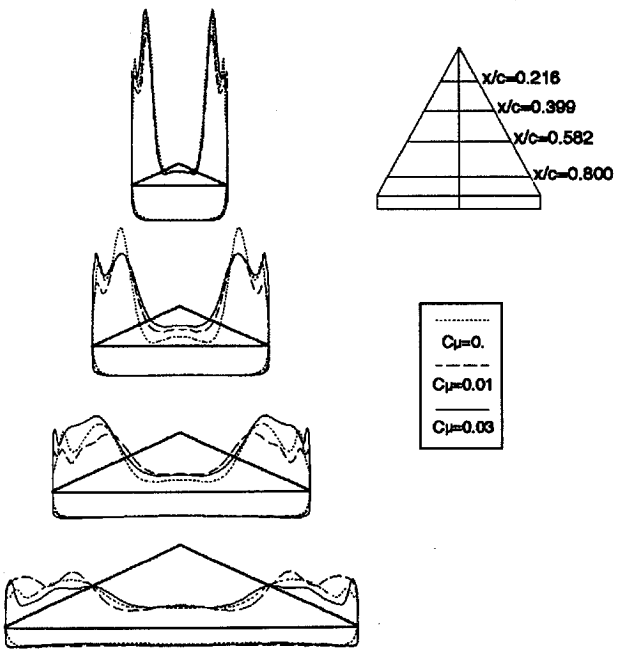

Fig. 11 Computed surface pressure distribution (α = 30 deg).

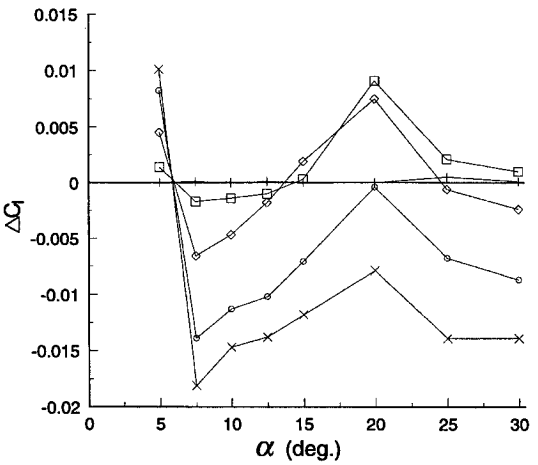

Fig. 12 Experimental results of rolling moment generation: +, C_μ = 0; □, C_μ = 0.01; ◇, C_μ = 0.03; ○, C_μ = 0.06; and ×, C_μ = 0.09.

was implemented by blocking the forward portion of the existing blowing slot. This arrangement was to create the effect of an aileron when asymmetrical blowing was applied to the model. The remaining blowing area was approximately half of the fully exposed slot, although it was only $l/c = 0.287$ long. Note that, for a particular C_μ, the partial blowing case had a mass flow rate of 0.707 times smaller than the full slot case. At $\alpha = 10$ deg, the effect of partial blowing on the rolling moment coefficient was approximately the same as compared with full blowing, as shown in Fig. 14. However, for $\alpha = 20$ deg, even though partial slot blowing uses less mass flow due to its smaller jet slot area, it was more effective than the full slot case in generating rolling moments. Furthermore, the blowing coefficient range where control reversal occurs was smaller for partial blowing, making the rolling moment generation more suitable for control purposes as demonstrated in Fig. 15. The effectiveness of the partial blowing was also captured and explained by the computational results. The computed pressure distributions in Fig. 16 indicate that full slot blowing strengthens the vortex along the entire leading edge of the wing, which in turn builds up the adverse

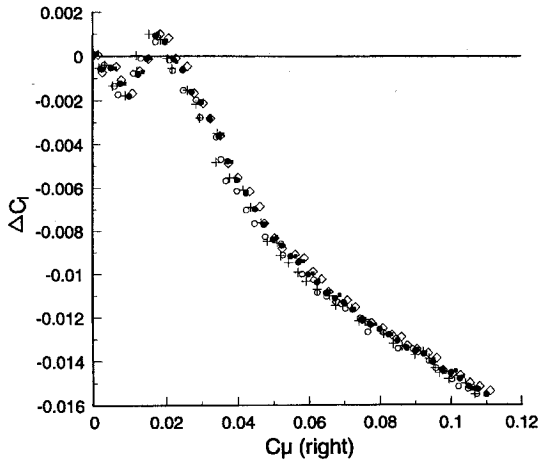

Fig. 13 Experimental results of rolling moment generation at different bank angles (α = 12.5 deg): ●, ϕ = 2 deg; ○, ϕ = 4 deg; ■, ϕ = 6 deg; +, ϕ = 8 deg; and ◇, ϕ = 10 deg.

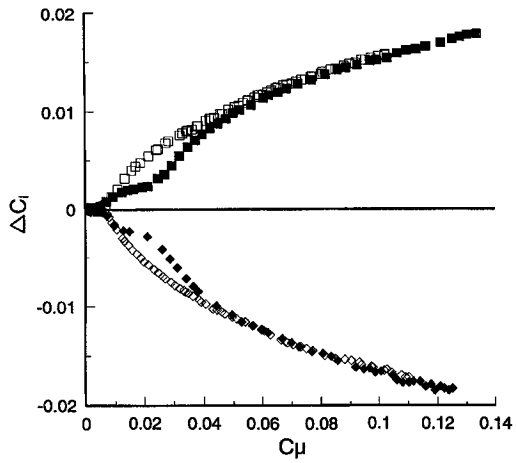

Fig. 14 Experimental results on the comparison of partial and full slot blowing (α = 10 deg). Full slot: ■, left-hand side and ♦, right-hand side. Partial slot: □, left-hand side and ◇, right-hand side.

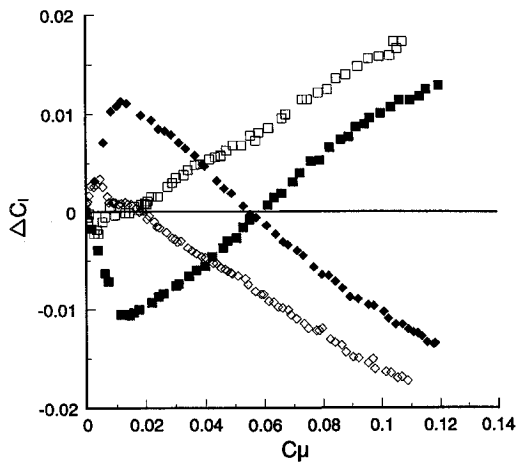

Fig. 15 Experimental results on the comparison of partial and full slot blowing (α = 20 deg). Full slot: ■, left-hand side and ♦, right-hand side. Partial slot: □, left-hand side and ◇, right-hand side.

pressure gradient along the core. Consequently, the vortex breaks down near the trailing edge, where the moment arm is long, and there is a large loss of suction peak. For the partial slot configuration, there is no change in the pressure distribution near the apex where no blowing is applied. However, this disadvantage is compensated by the large suction peak near the trailing edge. The partial slot is effective because it wastes no jet momentum near the apex where the moment arm is small. Furthermore, simple analysis shows that even though the partial slot has a mass flow rate 0.707 times

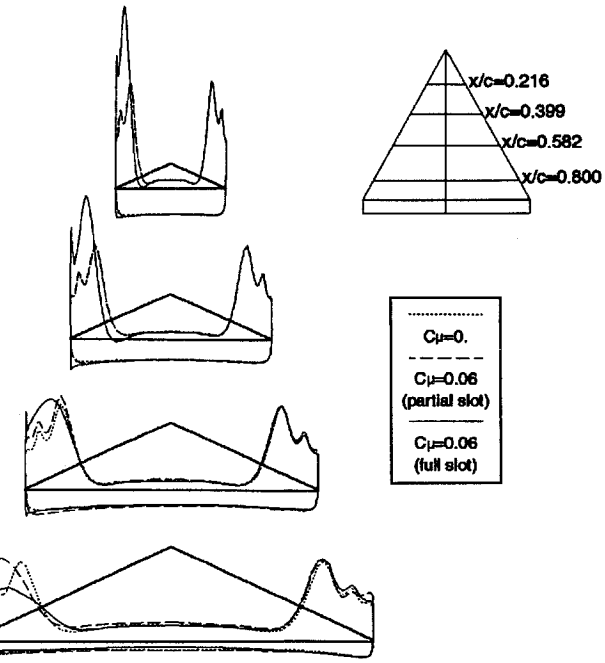

Fig. 16 Computed surface pressure distribution for full and partial slots (α = 20 deg).

smaller than the full slot case, the roll moment from the direct jet contribution is 29% larger than the full slot case.

Conclusions

An experimental and computational study has been conducted to explore the effects and the mechanics of lateral blowing to augment normal force and to provide roll control on a delta wing. It was demonstrated that the vortical flow over a wing could be manipulated by blowing symmetrically or asymmetrically. As expected, the normal force increases with the strength of the blowing jets. The aerodynamic forces and moments were found to be augmented by lateral blowing in three ways. First, the vorticity from the blowing jet feeds into the leading-edge vortex and strengthens it. Second, because a jet sheet can sustain a pressure difference, lateral blowing effectively increases the wing apex angle and hence the strength of the leading-edge vortex. Finally, there is a contribution from the direct jet momentum. The blowing scheme was shown to be equally effective for the range of angles of attack tested, except in the vicinity of 20 deg. At this transition angle, the normal force does not increase but decreases as the blowing is applied. The mechanism of this undesirable control reversal effect was determined by examining the experimental and computational results. For low angles of attack, lateral blowing augments the vortex strength, which gives an increase in vortical lift. However, the blowing scheme also aids vortex breakdown to move upstream, and therefore at certain angles of attack, there is a loss of lift, although, for high angles of attack, lateral blowing increases the area where the vortex is effective and compensates for the loss of suction peak due to the burst vortex. To obtain the desired forces and moments as efficiently as possible, the effect of blowing slot length was also studied. The experiments and computations show that even though the partial slot uses half of the area of the full slot and hence less mass flow, it is more effective than the full slot in generating roll moments for a large range of blowing strengths and angles of attack. Full slot blowing generates a moderately strong vortex along the leading edge, but for high blowing coefficients the vortex breaks down. However, partial slot blowing generates a very strong vortex near the trailing edge where the moment arm is long and is, therefore, a more efficient way to generate rolling moments.

Acknowledgment

This research was supported by Grant NCC 2-55 from the NASA Ames Research Center.

References

[1]Alexander, A. J., "Experiments on a Delta Wing Using Leading Edge Blowing to Remove Secondary Separation," College of Aeronautics, Rept. 161, Cranfield, England, UK, May 1963.

[2]Alexander, A. J., "Experimental Investigation on a Cropped Delta Wing with Edge Blowing," College of Aeronautics, Rept. 162, Cranfield, England, UK, June 1963.

[3]Trebble, W. J. G., "Exploratory Investigation of the Effects of Blowing from the Leading Edge of a Delta Wing," Aeronautical Research Council, R&M 3518, London, April 1966.

[4]Barsby, J. E., "Calculations of the Effect of Blowing from the Leading Edges of a Slender Delta Wing," Aeronautical Research Council, R&M 3692, London, April 1971.

[5]Tavella, D. A., "Lift of Delta Wings with Leading-Edge Blowing," *Journal of Aircraft*, Vol. 25, No. 6, 1988, pp. 522–524.

[6]Tavella, D. A., and Roberts, L., "The Concept of Lateral Blowing," AIAA Paper 85-5000, Dec. 1985.

[7]Lee, C. S., Tavella, D. A., Wood, N. J., and Roberts, L., "Flow Structure and Scaling Laws in Lateral Wing-Tip Blowing," *AIAA Journal*, Vol. 27, No. 8, 1989, pp. 1002–1007.

[8]Yeh, D. T., "Numerical Simulation of the Flowfield over Delta Wings with Leading Edge Blowing," Ph.D. Thesis, Dept. of Aeronautics and Astronautics, Stanford Univ., Stanford, CA, 1988.

[9]Celik, Z. Z., and Roberts, L., "Vortical Flow Control on a Delta Wing by Lateral Blowing," AIAA Paper 94-0509, Jan. 1994.

[10]Hong, J. S., and Roberts, L., "A Computational Study on the Effects of Leading Edge Lateral Blowing on Delta Wing Aerodynamics," AIAA Paper 95-1842, June 1995.

[11]Buning, G. B., Chan, W. M., Renze, K. J., Sondak, D. L., Chiu, I. T., and Slotnick, J. P., "OVERFLOW User's Manual," NASA Ames Research Center, Moffett Field, CA, Sept. 1993.

[12]Baldwin, B. S., and Lomax, H., "Thin-Layer Approximation and Algebraic Model for Separated Turbulent Flows," AIAA Paper 78-0257, Jan. 1978.

[13]Degani, D., and Schiff, L. B., "Computation of Supersonic Viscous Flows Around Pointed Bodies at Large Incidence," AIAA Paper 83-0034, Jan. 1983.

[14]Vinokur, M., "On One-Dimensional Stretching Functions for Finite Difference Calculations," *Journal of Computational Physics*, Vol. 50, Feb. 1983, pp. 215–234.